Available online at www.sciencedirect.com
ScienceDirect
Journal of Power Sources 160 (2006) 609–620
JOURNAL OF POWER SOURCES
www.elsevier.com/locate/jpowsour

Preparation and properties of new cross-linked polyurethane acrylate electrolytes for lithium batteries

P. Santhosh [a], T. Vasudevan [a], A. Gopalan [a,*], Kwang-Pill Lee [b]

[a] *Department of Industrial Chemistry, Alagappa University, Karaikudi-630 003, India*
[b] *Department of Chemistry Education, Kyungpook National University, Daegu 702-701, South Korea*

Received 9 August 2005; accepted 17 January 2006
Available online 27 April 2006

Abstract

A cross-linked polyurethane acrylate (PUA) is synthesized by end-capping a hexamethylene diisocyanate, hexamethylene diisocyanate/poly(ethylene glycol)-based prepolymer with hydroxy butyl methacrylate (HBMA). Significant interactions of lithium ions with the soft and hard segments of the host polymer are observed for the PUA complexed with lithium perchlorate ($LiClO_4$) by means of differential scanning calorimetry (DSC), and Fourier transform infra-red (FT-IR) spectroscopy measurements. The DSC results indicate the formation of transient cross-links with the ether oxygen of the soft segment and mixing of soft and hard phases induced by the Li^+ ions. The results of FT-IR spectroscopy and thermogravimetric analysis measurements support the formation of different types of complexes by interaction of Li^+ ions with different coordination sites of PUA. No detectable interactions are found between Li^+ ions and groups in HBMA. In addition, PUA follows the Arrhenius relationship for ion transport. Predominant formation of contact ion-pairs of $LiClO_4$ is observed through a.c. conductivity and DSC measurements. The lithium stripping–plating process is reversible and this implies better electrochemical stability over the working voltage range. Also, the PUA electrolyte shows better compatibility with lithium metal as inferred from impedance measurements and has a good cationic transference number that is suitable for the material to be used as a solid polymer electrolyte. Addition of HBMA into the PU matrix improves the tensile strength of the cross-linked PUA. Swelling measurements of PUA with plasticizer indicate better dimensional stability. A cell is constructed with PUA as the electrolyte and its performance is evaluated.

Keywords: Polyurethane acrylate; Cross-linking; Solid polymer electrolyte; Lithium-ion battery; Cationic transference number; Tensile strength

1. Introduction

Polymer electrolytes have been widely studied due to their applicability for a variety of solid-state and electrochemical device applications including batteries, fuel cells, supercapacitors, electrochromic devices, and chemical sensors [1–4]. After a successful technical feasibility conducted by Armand et al. [5], polymer electrolytes started to play an important role in developing new types of rechargeable lithium or lithium-ion batteries [6,7]. Today, special interest is focused on polymer electrolytes that have high performance at ambient and sub-ambient temperatures.

It has been found that polymer electrolytes based on host polymer matrices that have oxyethylene chains yield higher ionic conductivities only at elevated temperatures [8,9]. The semi-crystalline character and the high glass transition temperature are the reasons for the low conductivity at ambient temperature. On the other hand, gel polymer electrolytes (GPE) based on polyacrylonitrile [10,11], poly(vinylidene fluoride) [1,12] and poly(methyl methacrylate) [13,14] display higher ionic conductivity in the order of mS cm^{-1} at room temperature.

Recent reports [15–19] have documented that polyurethane (PU)-based polymers can be used as a polymer electrolyte for rechargeable lithium-ion batteries. The interest in using PU as a matrix for polymer electrolytes is related to the possibility of increasing the mechanical strength of linear polyethers. Furthermore, the low glass transition temperature (T_g) and hence higher segmental motion of the polyether soft segments leads to higher mobility of the dissolved ions. The hard segment domains, which

* Corresponding author. Tel.: +91 4565 228836; fax: +91 4565 225202.
E-mail address: algopal_99@yahoo.com (A. Gopalan).

0378-7753/$ – see front matter © 2006 Elsevier B.V. All rights reserved.
doi:10.1016/j.jpowsour.2006.01.091

are in the glassy state and either distributed or interconnected throughout the rubbery phase of the soft segment, act as reinforcing filler and hence contribute to the dimensional stability of the polymer electrolyte.

It can be concluded from earlier reports [15–19] that PU-type polymer electrolytes with –(CH_2–CH_2–O)– units display better conductivity compared with other analogues. Nevertheless, the dimensional stability of the electrolyte must be still improved for these materials to become practically viable. Cross-linking of some of the units as side chains is one of the various ways to improve the mechanical properties of a given polymer [20]. The cross-linked polymer has better phase-separation of the hard and soft segments. The mechanical properties of a well phase-separated material are superior to those of a poorly phase-separated material.

Systematic studies of urethane acrylate UV-curable materials were carried out by Copper and co-workers [21]. Kim et al. [20] have studied the electrochemical and electrical properties of a PUA–$LiCF_3SO_3$ system by means of a.c. impedance spectroscopy. Sun et al. [22] reported the mechanical properties of urethane cross-linked poly(ethylene oxide-co-propylene oxide) glycerol ether-plasticizer (tetraethylene glycol dimethyl ether, or methyl formamide) salt-$LiClO_4$-based polymer electrolytes. They found that the elastic modulus and tensile strength of the materials unexpectedly decreased with increasing salt concentration. This may be due to the predominance of intra-molecular coordination of the Li^+ ions by the polymer.

A cross-linked polyurethane acrylate (PUA) end-caped with hydroxy ethyl acrylate (HEA) has been reported [23]. The interactions of lithium ions with the soft and hard segments of the host PUA polymer were observed by means of differential scanning calorimetry (DSC), FT-IR spectroscopy and ^{7}Li MAS NMR spectroscopy. A series of cross-linked PUAs were synthesized using 4,4′-methylene bis(phenyl isocyanate), poly(ethylene glycol) (PEG) hydroxyl methacrylate and different reactive vinyl and divinyl diluents [24]. The electrolytes were prepared by UV radiation induced cross-linking of the PUA–diluent mixture. Depending upon the composition, these electrolytes exhibited a wide range of mechanical and electrical properties and showed good compatibility with Li electrodes.

In the present study, polyurethane containing –(CH_2–CH_2–O)– units have been cross-linked by reacting the end groups of the PU prepolymer with hydroxy butyl methacrylate (HBMA) and subsequently polymerized. Typically, a cross-linked polyurethane acrylate (PUA) is synthesized by end-capping a hexamethylene diisocyanate, hexamethylene diisocyanate (HDI)/PEG-based prepolymer with hydroxy butyl methacrylate (HBMA) followed by thermal cross-linking. Systematic characterization studies of the cross-linked PUA in the presence of $LiClO_4$ are made with DSC, FT-IR spectroscopy and a.c. impedance measurements to examine the phase transitions, interaction of Li^+ ions with segments of PUA, and conductivity in the cross-linked environment of PU. The electrochemical characteristics and applicability of the PUA as a solid electrolyte for rechargeable lithium batteries are also investigated.

2. Experimental

2.1. Materials

Poly(ethylene glycol) (PEG; molecular weight 400; E. Merck) was dehydrated under reduced pressure at 80 °C for 24 h before use. Hexamethylene diisocyanate (HDI), 1,4-buatane diol, hydroxybutyl methacrylate (HBMA) (Aldrich), 1,1′-azobis(cyclohexane carbonitrile) (Aldrich) and the commercial battery electrolyte, LP-20 (Merck) were used as-received. $LiClO_4$ (Aldrich) was dehydrated at 120 °C under reduced pressure for 72 h. All the other reagents and chemicals were used without further purification.

2.2. Synthesis of PUA

Polyurethane acrylate was synthesized by a two-step addition process, in which the prepolymer was made by reaction of excess of HDI with PEG and then the end NCO groups were capped by reaction with HBMA. The prepolymer was made by allowing a mixture of HDI and PEG to react at 85 °C for 6 h with constant stirring under a dry nitrogen blanket. After completion of the prepolymer formation (confirmed by estimation of NCO groups by the di-butyl amine back titration method), dimethyl formamide (DMF) was added to dissolve the prepolymer. The temperature of the mass was reduced to 60 °C and then the required amount of HBMA was slowly added to the reaction mixture. The reaction was allowed to continue for 2 h and then was terminated by the addition of 2 ml of methanol. The molar ratio of HDI, PEG and HBMA for this PUA was 2:1:2. The structure of the synthesized PUA is shown in Scheme 1.

2.3. Preparation of polymer electrolytes

Solid polymer electrolytes (SPE) were prepared by mixing various concentrations of $LiClO_4$ in DMF with a PUA solution in DMF. 1,1′-Azobis(cyclohexane carbonitrile) was also mixed with the PUA for thermal cross-linking through the acrylate end groups. After homogeneous mixing, the solution was cast into Teflon plates. Solvent removal and simultaneous cross-linking were done at 80 °C under reduced pressure for 72 h. The films were kept inside a glove box prior to experiment. An undoped film was also prepared in the same way (but with no $LiClO_4$) for swelling study in the liquid electrolyte LP-20.

2.4. Differential scanning calorimetry

The DSC experiments were carried out using a DSC 2010 differential scanning calorimeter (TA Instruments, USA) over the temperature range −150 to 150 °C at a scan rate of 10 °C min^{-1}. The dry samples were sealed in Al crucibles inside a glove box. The sealed samples were removed from the glove box immediately before the DSC experiments. The samples were first annealed at 150 °C for 10 min, cooled to −150 °C, and then scanned. All the thermograms were base-line corrected and calibrated against Indium metal. The glass transition temperature

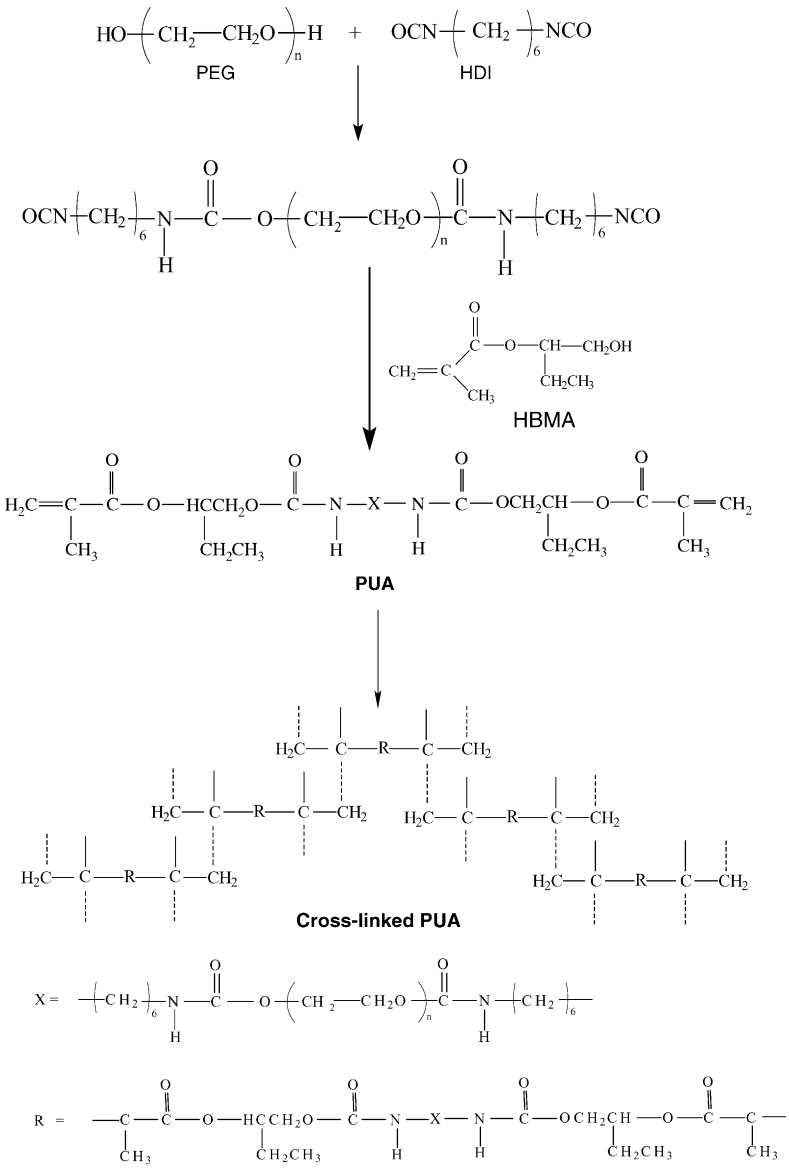

Scheme 1. Schematic representation of synthesis of PUA.

(T_g) is reported as the midpoint of the transition process and the melting temperature is the peak temperature.

2.5. Fourier transform infra-red spectroscopy

FT-IR spectra were taken at ambient temperature using a Perkin-Elmer Rx1 instrument with a wave number resolution of 4 cm^{-1}. Samples for FT-IR analysis were made by casting the polymer–salt mixture directly on to KBr pellets and then simultaneously drying them at 120 °C for 48 h. About 125 scans were signal averaged to increase the s/n ratio. Data processing was performed by Grams 386 software (Galactic Industries Corporation).

2.6. AC impedance measurements

Impedance measurements of the polymer electrolytes were performed using thin films made by casting from solution and drying. Film thicknesses were maintained in the range 250–350 μm and the area of contact was 1.0 cm^2. For measurement of ionic conductivity, the samples were sandwiched between two stainless-steel (SS) electrodes. Cell assembly was carried out in dry argon atmosphere inside a glove box. Conductivity measurements were performed using a EG & G PAR 6310 Potentiostat/Galvanostat controlled by frequency response analysis under an oscillation potential of 10 mV. The conductivity was calculated from the relation:

$$\sigma = \frac{1}{R_b}\frac{\lambda}{A} \quad (1)$$

where R_b is the bulk resistance obtained from the alternating current impedance, λ the film thickness, and A is the surface area of the electrode.

2.7. Cyclic voltammetry and linear sweep voltammetry

Cyclic voltammetry (CV) and linear sweep voltammetry (LSV) were performed with a cell made by using stainless steel (SS 304) as a working electrode and Li metal as a counter as well as a reference electrode. The CV experiments were performed in the potential range of −0.5 to 4.0 V (versus Li). For LSV, the potential of the working electrode was varied from 2.0 to 6.0 V (versus Li). A sweep rate of 5 mV s^{-1} was used in both cases. Electrochemical measurements were made using a Bio Analytical System 100 B (BAS 100BW) Electrochemical Analyzer.

2.8. d.c. Polarization measurement

A d.c. polarization cell was constructed by sandwiching the electrolyte film between symmetrical lithium metal electrodes. A small constant potential difference of about 10 mV was applied across a symmetric cell and the current was measured as a function of time until it reached a constant value. By considering the potential drop in the surface layers on the electrode, the cation transport number t_+ was determined by using the relation [25]:

$$t_+ = \frac{I_{ss}(\Delta V - I_i R_i)}{I_i(\Delta V - I_{ss} R_{ss})} \quad (2)$$

where I_i and I_{ss} are the initial and steady-state currents, R_i and R_{ss} are the initial and steady-state resistance of the passivating layers, and ΔV is the applied potential. The impedance spectra were recorded before and after the current relaxation measurement without interruption of the d.c. bias, to permit R_i and R_{ss} to be evaluated.

2.9. Thermogravimetric analysis

Thermogravimetric analyses (TGA) of the prepared polymer electrolyte samples were performed under nitrogen atmosphere using a Perkin-Elmer TGA 7/DX Thermal Analyzer with a scan rate of 20 °C min^{-1}.

2.10. Mechanical strength

Tensile strength was measured at room temperature by means of a Universal tensile machine (Instron model 5565, Lloyd) at a full-out velocity of 50 mm min^{-1}. The polymer electrolyte sample thickness was 100 μm. Measurements were performed five times for each sample, and the average value was calculated.

2.11. Charge–discharge cycling tests

$LiCoO_2$ and Li were employed as the cathode and the anode, respectively. The area of both electrodes was fixed as 2.0 cm^2. Li/PE/$LiCoO_2$ laminated cells were assembled by pressing Li, PE and $LiCoO_2$, which were sealed by a polyethylene film and laminated by an aluminium foil. The charge–discharge cycling tests of the laminated cell electrolyte were conducted under galvanostatic conditions in a dry argon atmosphere.

Table 1
DSC data for PUA with different $LiClO_4$ concentration

Film	T_g SS (°C)	$\Delta T_g/\Delta C$ (°C mM^{-1} g^{-1})	T_g HS (°C)	T_m (°C)
0	−60.0	–	+79.8	42
a	−58.4	19.5	+75.6	–
b	−49.2	22.6	+70.0	–
c	−30.6	28.0	+60.4	–
d	−20.0	32.2	+48.2	–
e	−14.9	27.6	+73.0	–
f	−12.1	25.0	+79.1	–

Film of PUA doped with different concentration of $LiClO_4$: (0) PUA, (a) 0.10 mM g^{-1} PUA, (b) 0.15 mM g^{-1} PUA, (c) 0.20 mM g^{-1} PUA, (d) 0.40 mM g^{-1} PUA, (e) 0.50 mM g^{-1} PUA and (f) 0.75 mM g^{-1} PUA.

3. Results and discussion

3.1. Differential scanning calorimeter

The effect of $LiClO_4$ on the morphology-based thermal transitions of PUA, as well as the polyether soft segment T_g, were examined by DSC. Table 1 presents the DSC results of the undoped and $LiClO_4$ doped cross-linked PUA. The parent undoped PUA shows a crystalline endothermic peak at 42 °C and a low-temperature endothermic transition at −60 °C. These two transitions correspond to the melting of the crystalline region (T_m) and the liquid–glass transition of the amorphous region of PEG in the soft segment (T_g SS). The T_g of the polyether (PEG-400) used in this study was noted at −56 °C. As can be seen from Fig. 1(A), the variation of the soft segment T_g increases as a function of salt concentration. This is consistent with previous investigations on $LiClO_4$ doped TPU having PEG [26,27] or PPO [28,29] as the soft segment. The PEG soft segment partially arrests the local motion of the polymer segments through the formation of transient cross-links which result in an increase in the soft segment T_g. Also, stiffening of the polyether chains due to the ion–dipole interaction between Li^+ ions and the polyether oxygen is expected.

By normalizing the T_g data with respect to salt concentration, $\Delta T_g/\Delta C$ was calculated and a non-linear increase in T_g could be observed with increase in concentration. The $\Delta T_g/\Delta C$ value reaches a maximum at [$LiClO_4$] 0.40 mM g^{-1} PUA and thereafter shows a decreasing trend (Table 1 and Fig. 1(B)). This may probably be due to the plasticizing effect created by the formation of charge-neutral contact ion-pairs with increasing salt concentration [30]. The neutral contact ion-pairs lack the ability to form cross-links, and hence cannot increase the T_g. Conductivity measurements also predict ion-pair formation beyond [$LiClO_4$] 0.40 mM g^{-1} PUA. This is discussed below.

The second thermal event, at approximately 70 °C for the pure polymer, may be attributed to an endothermic process for the aliphatic hard segment (HS). Addition of salt results in changes in the T_g of HS, but without displaying any trend with salt concentration. This endotherm was initially interpreted as being associated with hydrogen bond dissociation, but was discussed later in terms of morphological behaviour [31–33]. It has been proposed that this might be due to the loss of order close to

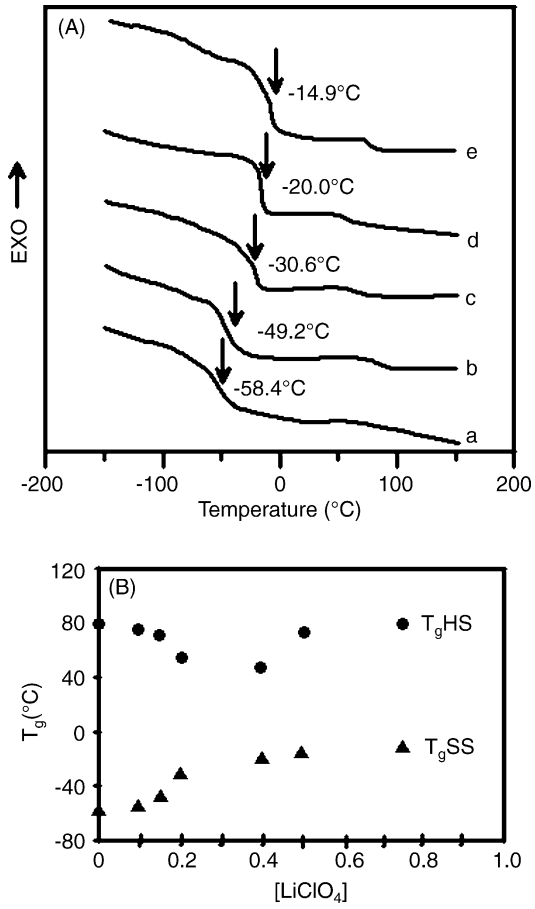

Fig. 1. (A) DSC thermograms of PUA doped with various $LiClO_4$ concentrations. (a) 0.10 mM g^{-1} PUA, (b) 0.15 mM g^{-1} PUA, (c) 0.20 mM g^{-1} PUA, (d) 0.40 mM g^{-1} PUA and (e) 0.50 mM g^{-1} PUA. (B) Variation of soft segment and hard segment T_g of PUA with salt concentration.

the hydrocarbon chains of HS, but not involving hydrogen bond dissociation. It is evident from the date in Table 1 that the T_g of HS tends to decrease with increase in salt concentration up to [$LiClO_4$] 0.4 mM g^{-1} PUA. This may be due to the phase mixing of hard and soft segments in PUA in the presence of $LiClO_4$. In the presence of $LiClO_4$, the crystalline structure of PEG in doped PUA may be disrupted and may be the reason for the absence of the peak corresponding to crystalline regions. This indicates that doped PUA is transformed fully into the amorphous form by addition of the salt.

Due to the presence of different coordination sites in the PUA system, various types of complexes can be formed by the interaction of coordination sites with Li^+ ions. Three major types of interactions can be distinguished [16], namely: (i) interaction of the ether oxygen with Li^+ ions, as mentioned earlier, leading to the formation of transient cross-links between the polyether chains via Li^+ ions, which restrict the segmental motion; (ii) interaction of urethane –NH and carbonyl groups with Li^+ ions to give inter- or intra-molecular cross-linking; (iii) mixed ether–urethane interactions with Li^+ ions leading to phase mixing of the hard and soft segments.

Three types of complexes that arise out of the above three interactions are shown in Scheme 2. The formation of such

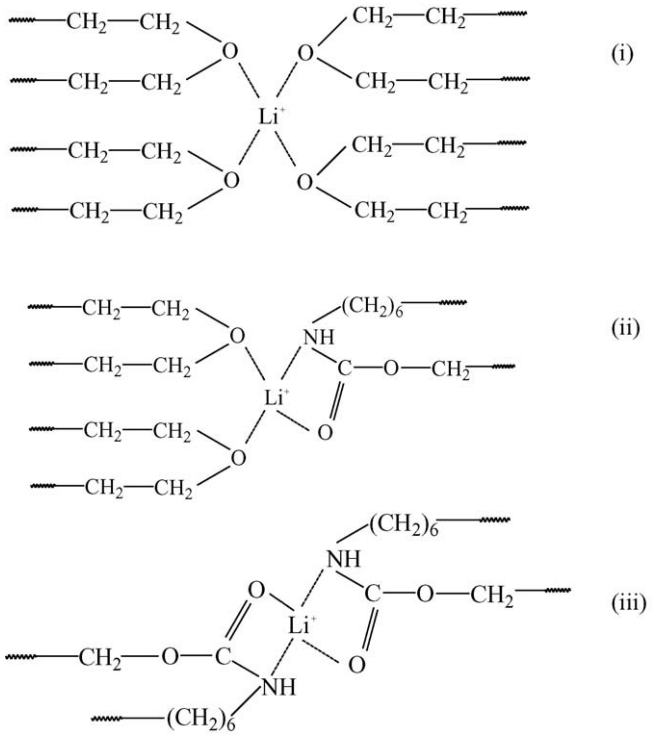

Scheme 2. Interaction of Li^+ ions PUA.

complexes has been reported earlier for composite systems such as PEO-poly(vinyl pyridine)-$LiClO_4$ [34] and PEO-poly(*N*,*N*-dimethyl acrylamide)-$LiClO_4$ [35].

3.2. FT-IR spectroscopy

FT-IR spectroscopy has been conducted at ambient temperature to examine the effects of alkali metal salt concentration on the interaction of Li^+ ions with groups in the PUA. One typical spectrum of undoped PUA is shown in Fig. 2. In order to gain an insight into the effect of Li^+ ions on the H-bonding interac-

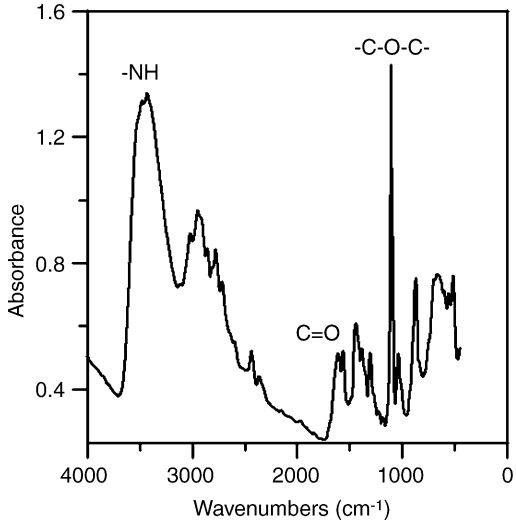

Fig. 2. FT-IR spectrum of undoped PUA.

tions of the hard and soft segments, three regions of the FT-IR spectrum have been chosen, namely:

(1) 4000–3000 cm^{-1}, the region for free and H-bonded –NH stretching modes;
(2) 1800–1600 cm^{-1}, the region for urethane carbonyl symmetric stretching vibrations;
(3) 1200–1100 cm^{-1}, the region for C–O–C stretching of PEG, C(O)–O–C stretching of the hard segment and C(O)–O–C stretching of the acrylate group.

3.2.1. 4000–3000 cm^{-1} region

The –NH stretching region of the FT-IR spectra is characterized by four modes of vibrations [36]. The relative IR absorbance in the –NH stretching region for undoped PUA and PUA doped with 0.4 mM $LiClO_4$ g^{-1} PUA is shown in Fig. 3. The inset shows the deconvolution of the –NH stretching region for undoped PUA and the results are given in Table 2. Four IR regions have been examined from the Fig. 3 (inset) and assigned [33,36], viz.,

(i) 3587 cm^{-1}, the peak in the region includes the free –NH and hydrogen-bonded –NH stretching vibrations;
(ii) 3574 cm^{-1}, the peak in the region includes the overtones of the carbonyl group;
(iii) 3505 cm^{-1}, the peak in the region includes the H-bonded –NH stretching formed with the carbonyl group;
(iv) 3396 cm^{-1}, the peak in the region includes the H-bonded –NH stretching formed with the ether oxygen.

An examination of the data in Table 2 indicates that all the peaks undergo a shift towards lower frequency when doped with $LiClO_4$. This feature is due to the possible interactions of Li^+ ions with the different coordination sites of PUA, as shown in Scheme 3. The shifting of the free –NH band position to the lower frequency in the presence of $LiClO_4$ may be attributed to coordination of Li^+ ions to the nitrogen atoms of the free –NH groups (Scheme 3(a)). The two H-bonded peaks also move towards lower frequency after the addition of $LiClO_4$. Shifting of the H-bonded –NH band positions to lower frequency can be explained by Schemes 3(b) and (c). The respective peak areas for all the –NH bands are given in Table 2. The peak areas are normalized against the total –NH band area. As the absorptiv-

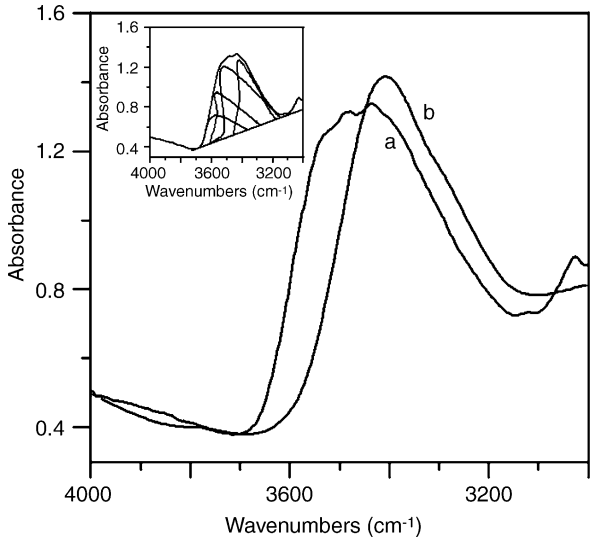

Fig. 3. Relative IR absorbance in –NH stretching region for undoped PUA and a PUA doped with 0.4 mM $LiClO_4$ g^{-1} PUA (inset shows deconvolution of –NH stretching region for undoped PUA).

Table 2
Deconvolution data of FT-IR spectra of PUA in –NH stretching region

Sample	$LiClO_4$ (mM g^{-1} PUA)	Peak positions (cm^{-1})				Percent area[a]			
		1	2	3	4	1	2	3	4
0	0.00	3587	3574	3505	3396	11.2	28.4	35.1	25.3
A	0.10	3554	3548	3472	3341	16.5	25.2	37.3	21.1
B	0.15	3536	3520	3454	3290	28.3	20.5	38.7	12.5
C	0.20	3514	3501	3421	3212	30.6	15.6	42.3	10.9
D	0.40	3495	3483	3400	3180	31.9	14.1	45.8	8.2

Peak 1, free –NH bonding; peak 2, overtone of C=O; peak 3, hard–hard segment H-bonding; peak 4, hard–soft segment H-bonding.
[a] Peak areas are based on total –NH stretching band area.

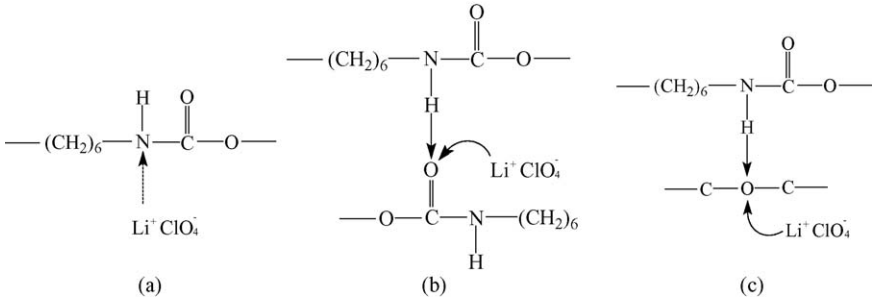

Scheme 3. Interaction of Li^+ ions to –NH group of PUA.

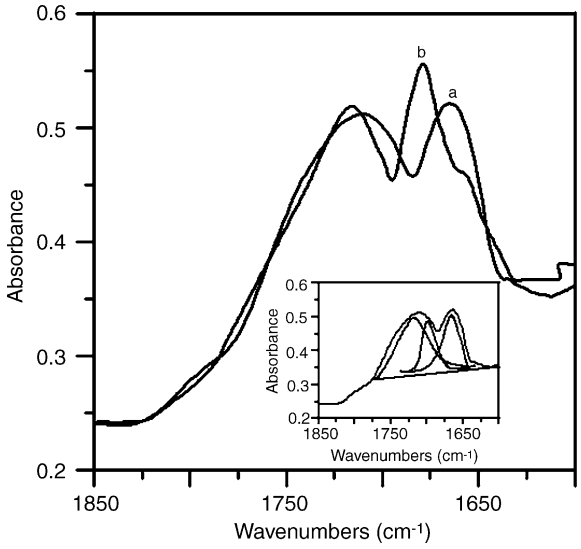

Fig. 4. Relative IR absorbance in C=O stretch region for undoped PUA and a PUA doped with 0.4 mM $LiClO_4$ g^{-1} PUA (inset shows deconvolution of C=O stretching region for undoped PUA).

ity coefficient of –NH groups in a TPU is reported [37,38] to be a strong function of strength of the H-bonds and the band frequency, quantitative measurement of the free and H-bonded –NH groups is not possible from the peak area values. Nevertheless, a qualitative assessment can be made of the relative extent of interaction of Li^+ ions with the hard and soft segments [39]. It is evident from the area values that the extent of –NH groups H-bonded to the ether oxygen is more in the absence of Li salt (Table 2). In the presence of Li salt, the number of –NH groups H-bonded to the carbonyl oxygen becomes higher. With the addition of salt, the Li^+ ions preferentially coordinate to the easily accessible ether groups and hence reduced the extent of –NH groups that are hydrogen bonded to ether groups.

3.2.2. 1800–1600 cm^{-1} region

The relative IR absorbance in the carbonyl stretching region for undoped PUA and PUA doped with 0.4 mM $LiClO_4$ g^{-1} PUA is shown in Fig. 4. The inset shows the deconvolution of the carbonyl stretching region for undoped PUA and the results are given in Table 3. The deconvoluted FT-IR spectra of the undoped and the doped samples are used to obtain the percent areas (Table 3) for the carbonyl stretching vibrations. Three modes of vibration are visualized, i.e., the free or non-H-bonded

Table 3
Deconvolution data of FT-IR spectra of PUA in C=O stretching region

Sample	$LiClO_4$ (mM g^{-1} PUA)	Peak positions (cm^{-1})			Percent area[a]		
		1	2	3	1	2	3
0	0.00	1725	1695	1662	34.3	35.3	30.4
1	0.10	1722	1692	1668	32.2	33.1	34.5
2	0.15	1719	1687	1672	28.1	30.3	41.6
3	0.20	1715	1685	1676	25.7	28.2	46.1
4	0.40	1710	1704	1680	21.3	26.4	52.2

Peak 1, free carbonyl; peak 2, disordered H-bonded carbonyl; peak 3, ordered H-bonded carbonyl.
[a] Peak areas are based on total C=O stretching band area.

C=O (1725–1710 cm^{-1}) and two stretching vibrations associated with disordered (1695 cm^{-1}) and ordered (1662 cm^{-1}) H-bonded C=O [40]. It is apparent from Table 3 that the three peaks are shifted to lower frequency by the addition of Li salt. This may be attributed to the coordination of electron deficient Li^+ ions with carbonyl oxygen atoms, which weakens the C=O bond by sharing the electron density of the carbonyl oxygen atoms.

3.2.3. 1200–1000 cm^{-1} region

The relative IR absorbance in the ether stretching region for undoped PUA and PUA doped with 0.4 mM $LiClO_4$ g^{-1} PUA is presented in the Fig. 5 and the results are given in Table 4.

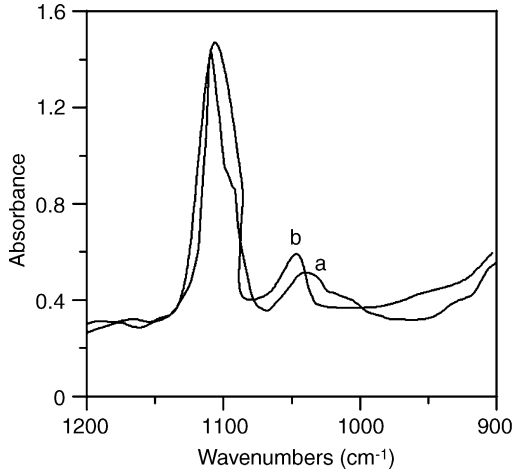

Fig. 5. Relative IR absorbance in ether stretching region for undoped PUA and a PUA doped with 0.4 mM $LiClO_4$ g^{-1} PUA.

Table 4
Deconvolution data of FT-IR spectra of PUA in ether stretching region

Sample	$LiClO_4$ (mM g^{-1} PUA)	Peak positions (cm^{-1})				Percent area[a]			
		1	2	3	4	1	2	3	4
0	0.00	1100	1090	1045	1010	22.2	32.5	35.2	9.7
a	0.10	1102	1085	1039	1005	25.3	27.9	40.8	5.8
b	0.15	1101	1079	1035	1001	32.5	26.8	37.5	3.2
c	0.20	1100	1075	1031	998	41.5	20.2	35.2	2.8
d	0.40	1098	1071	1050	995	49.2	18.6	31.1	1.1

Peak 1, C(O)–O–C stretch of the acrylate; peak 2, C–O–C stretch of PEG; peak 3, C(O)–O–C stretch of the urethane; peak 4: H-bonded C–O–C stretch of PEG.
[a] Peak areas are based on total ether stretching band area.

The deconvoluted FT-IR spectra of the undoped and doped PUA samples show four characteristic vibrational modes (Table 4), namely:

(1) the peak at 1100–1098 cm^{-1} is assigned to C(O)–O–C stretching of the acrylate groups [39]
(2) the second peak at 1090–1071 cm^{-1} is assigned to the C–O–C stretching of PEG
(3) the peak at 1045 cm^{-1} is due to C(O)–O–C stretching of the urethane groups
(4) the fourth peak at 1010–995 cm^{-1} is assigned to H-bonded C–O–C stretching of PEG [40].

The data in Table 4 show that there is no obvious change in the position of the acrylate C(O)–O–C stretching band on adding lithium salt. The bands of C(O)–O–C and C–O–C stretching of the urethane groups experience only a marginal shift to lower frequencies on the addition of lithium ions. A comparison of the percent area (Table 4) reveals that on adding the salt, some of the H-bonded C–O–C groups become free. This may be due to the interaction of Li^+ ions with the ether oxygen leading to a decrease in the electron density of this oxygen and in its ability to form H-bonds. All these observations indicate that the introduction of Li salt into PUA results in various types of interaction that cause a change in the microstructure of the polymer.

3.3. Ionic conductivity

Cross-linking of the polymer electrolyte is expected to result in better mechanical stability, a lower degree of crystallinity, and a lower T_g and thus higher ionic conductivity [41]. The ionic conductivity of a polymer electrolyte depends on the effective number of carrier ions and the ion mobility. The effective number of carrier ions is related to the concentration of the dissolved ions. The ion mobility in a polymer electrolyte formed by the dissolution of ions in the polymer is facilitated by the segment mobility of the polymer chains. Values of the ionic conductivity obtained from a.c. impedance measurements are given in Fig. 6(A) as a function of $LiClO_4$ concentration. An increase in conductivity with salt concentration is observed and a maximum conductivity (0.75×10^{-5} S cm^{-1} at 35 °C) is obtained at a salt concentration of [$LiClO_4$] 0.4 mM g^{-1} PUA.

Generally, conductivity increases with salt concentration. In the case of PUA, however, the conductivity increases rapidly with salt concentration, reaches a maximum at [$LiClO_4$] 0.4 mM g^{-1} PUA, and thereafter decreases. This may be due to the interaction of two opposite effects, namely, an increase in the number of charge carriers [42] and a decrease in the free volume [43,44]. The number of charge carriers is increased as the concentration of salt is increased. On the other hand, the average free-volume is decreased due to the increase in T_g (as a result of the interaction of Li^+ ions with the ether oxygen). At a low concentration of salt, the increase in the number of charge carriers dominates, whereas at a high salt concentration, the reduction in free-volume takes precedence [45]. When the salt concentration reaches [$LiClO_4$] 0.4 mM g^{-1} PUA or more, the decrease in free-volume becomes more pronounced than the increase in number of charge carriers. At this stage, the lower fraction of free-volume is no longer compensated by the continuous increase in the number of charge carriers. As a result of which, the conductivity is decreased with increase in salt concentration at a high salt concentration level. Additionally, at such salt concentrations a considerable amount of salt remains as ion-pairs, that do not contribute to the conductivity of the electrolyte.

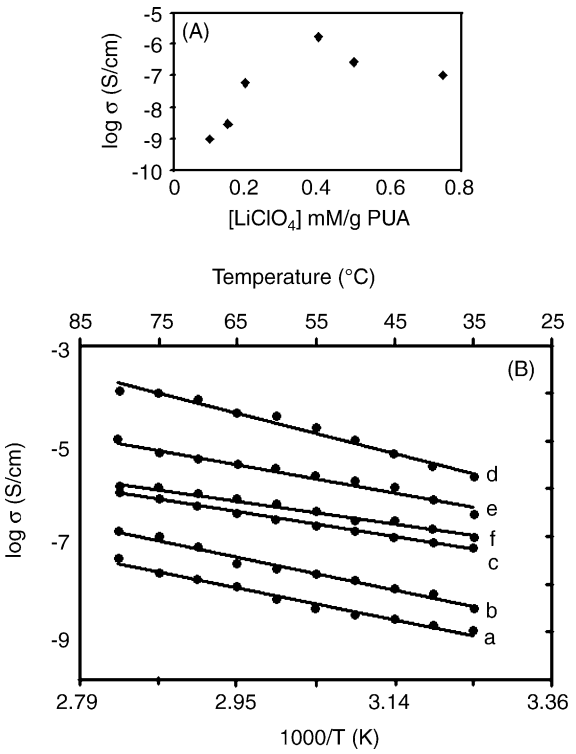

Fig. 6. (A) Variation of conductivity of PUA electrolyte with $LiClO_4$ concentration at 35 °C. (B) Temperature dependence of ionic conductivity of PUA doped with different amount of $LiClO_4$. (a) 0.10 mM g^{-1} PUA, (b) 0.15 mM g^{-1} PUA, (c) 0.20 mM g^{-1} PUA, (d) 0.40 mM g^{-1} PUA, (e) 0.50 mM g^{-1} PUA and (f) 0.75 mM g^{-1} PUA.

The ionic conductivity for various concentrations of $LiClO_4$ are plotted against the reciprocal of the temperature in Fig. 6(B). The PUA follows the Arrhenius relationship for ion transport. The data indicate that sample d ([$LiClO_4$] 0.4 mM g^{-1} PUA) has the highest conductivity at all the temperatures examined. This is due to higher number of charge carriers at higher salt concentrations. The lower value of samples e and f compared is ascribed to the increased ion-pair formation with increase in salt concentration. This observation is consistent with the results from DSC studies (Table 1).

3.4. Cyclic voltammetry studies

Cyclic voltammetry was performed to study the kinetics of the lithium deposition–stripping process of the PUA electrolyte. Repetitive cyclic voltammograms for a Li/PE/SS cell using PUA at ambient temperature are shown in Fig. 7. The sweep rate was as 5 mV s^{-1}. The trend of the voltammetric curves indicates that the process at the lithium interface is reversible in the PUA elec-

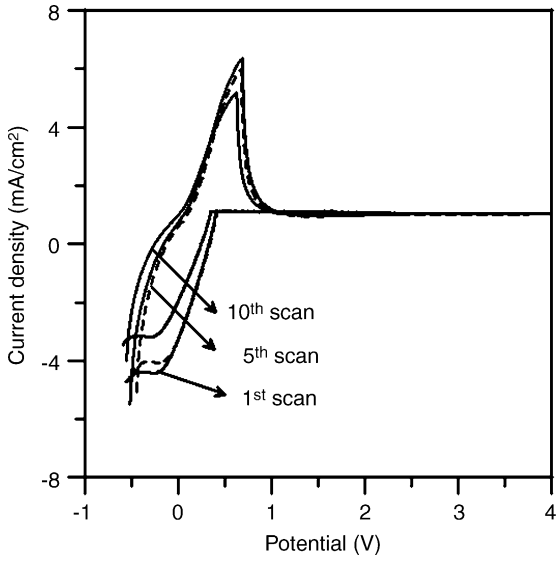

Fig. 7. Cyclic voltammograms of PUA. Scan rate, 5 mV s^{-1}.

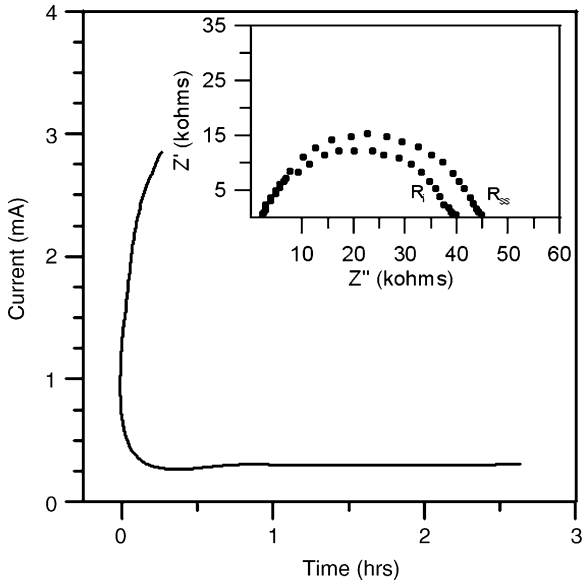

Fig. 8. Current relaxation plot for transport number measurement of PUA (inset: complex impedance plot: initial resistance and steady-state resistance measured before and after current transient).

trolyte medium. The cycleability is good and the recovery of lithium is high. On sweeping towards more negative potentials, a peak is observed at ∼−0.35 V versus Li and corresponds to the deposition of lithium on the SS electrode. On the reverse scan, stripping of lithium from the SS electrode is observed at ∼0.52 V. Although the process remains reversible on cycling, the amount of cycled lithium decreases progressively. This phenomenon may be attributed to the formation of a passive layer on the SS electrode, that is phenomenologically similar to those commonly experienced in liquid organic electrolytes. The formation of a passive layer is also confirmed by the impedance response of the lithium electrode in polymer electrolytic media. The reversible process in the electrolyte membrane demonstrates that the cross-linked PUA system is electrochemically stable and hence can be safely used as a polymer electrolyte in rechargeable lithium batteries.

3.5. Transport number

The transport number of an electrolyte is an important index of its conductive behaviour. Since the electrochemical process in lithium batteries involves the intercalation and de-intercalation of lithium cations throughout the host compound lattice, a solid polymer electrolyte with a cation transference number (t_+) approaching unity is desirable for avoiding a concentration gradient during repeated charge–discharge cycles. Thus, evaluation of the t_+ is of great importance for the characterization of polymer electrolytes.

The impedance response of a Li/PUA/Li cell, inset of Fig. 8, was monitored both initially and under steady-state current conditions. The observed decrease in current (Fig. 8) may be due to the formation of passivating layers on the electrode [46]. The current response is completely stabilized after 2 h. The t_+ value of the PUA is 0.52.

The reported t_+ values for dry polymer electrolytes range from 0.06 to 0.2 [47]. For gel polymer systems, t_+ values of the order 0.4–0.5 have been reported for poly(bis methoxy ethoxy ethoxy) phosphazene [48] and a value = 0.56 for PEO-PMMA systems [49]. The value of 0.52 found in this study is lower than that of a PAN-based (0.6–0.8) [50] or a PMMA-based gel electrolyte (0.5–0.7) [51]. Nevertheless, the t_+ of about 0.52 for PUA systems is acceptable for a solid polymer electrolyte.

3.6. Impedance spectra

The impedance spectra of a Li/PUA/Li cell at various times are exhibited in Fig. 9. As is well known, the resistance of a cell system is composed of the bulk resistance R_b and interfacial resistance R_i. The latter reflects the interfacial situation between the electrolyte and the electrode. If the electrolyte reacts with the electrode, R_i will increase rapidly with time. All the curves in Fig. 9 are similar in shape with arcs in the high-frequency region and straight lines in the low-frequency region. In the very low-frequency region, the diffusion of active species determines the impedance response. This is due to charging of the double-layer during potential oscillation with charge transfer between

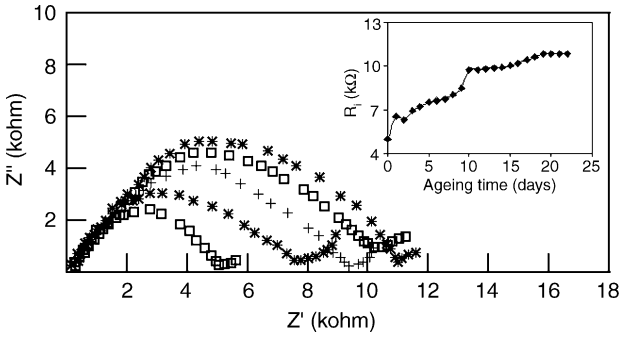

Fig. 9. Nyquist plot for cell with PUA as polymer electrolyte measured at different periods (inset: interfacial resistance behaviour of PUA at different periods).

the electrode surface and the electrolyte. As a consequence, a straight line is obtained in the Nyquist plot, this is the so-called 'Warburg diffusion impedance'. With increasing frequency, the charge-transfer reaction during potential oscillation decreases so that the influence of the diffusion of active species on the impedance response decreases.

It is inferred from the impedance plots in Fig. 9 that the diameter of the semicircle increases as a function of time. This can be attributed to the growth of a passivating film on the lithium surface. It is evident from Fig. 9 (inset) that the R_i values increase sharply to 6.5 kΩ during first 2 days and then show a slow increase with storage time. A value of 10.8 kΩ is reached after storing for more than 22 days. The continuous increase can be attributed to the role of the acrylate in PU towards stability. Acrylate can impart good adhesiveness to solid electrolytes and can make them stable in atmospheric moisture conditions [52,53]. In this case, acrylate helps to reduce the effect of moisture on the electrolyte and to retard the growth of a passivation film between the electrolyte and the lithium electrode. It is obvious from the impedance results that the PUA electrolyte exhibits good compatibility with lithium metal.

3.7. Electrochemical stability

The electrochemical stability window of a solid polymer electrolyte is generally determined by linear sweep voltammetry of an inert electrode in the selected electrolyte [54]. The onset of current at a high positive voltage is assumed to result from a decomposition process associated with the electrode [55] and this onset voltage is taken as the upper limit of the electrolyte stability range. This voltage is generally located at the point of intersection of the extrapolated linear current in the high-voltage region with the voltage axis.

To ascertain the electrochemical stability potential window for the PUA electrolyte, LSV was performed on a laminated electrode cell at ambient temperature. The potential was scanned from 1.0 to 6.0 V (versus Li/Li^+) at a sweep rate of 5 mV s^{-1}. The current–voltage curve of the PUA electrolyte cell is presented in Fig. 10. Two important features can be recognized from the trend of this curve. First, the current onset occurs at 5.35 V versus Li, which suggests that the electrolyte has a high anodic stability. The second notable feature is the very low current (0.5 μA cm^{-2}) prior to the onset of anodic breakdown. Above this cell voltage, the current increases steeply as the applied voltage is increased. This low residual current level up to 5.35 V with the absence of any peaks in the low voltage range confirms the high purity of the electrolyte. In particular, it is important to note that no peak is observed at 4.25 V versus Li, namely, at the voltage expected for the oxidation of water or any impurities [56].

3.8. Mechanical property

The stress–strain curve (Fig. 11) provides information on the mechanical properties of the PUA polymer electrolyte. For the comparative purposes, a PU electrolyte was synthesized and its mechanical properties determined. The strain of the electrolyte films varies markedly between the two electrolytes. A tensile strength (stress) as high as 4×10^3 kPa at an elongation-at-break value (strain) of 45% is observed of for the PU-based electrolyte, whereas a strain of 65% was noticed for the PUA-based electrolyte. The high elastic property of the PUA-based polymer electrolytes compared with its parent PU electrolyte is attributed to the chemically cross-linked network structure in the PUA electrolyte.

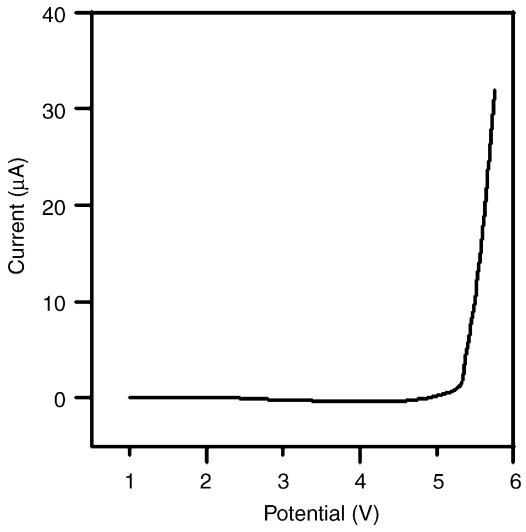

Fig. 10. Electrochemical stability of PUA performed by linear sweep voltammetry.

3.9. Thermal analysis

Typical TG curves for undoped and doped PUA electrolytes are shown in Fig. 12. The pure polymer decomposes in a single step beginning at 410 °C. The introduction of the salt promotes the decomposition of the PUA. The decreasing trend in the initial decomposition temperature (T_d) for the samples with increasing $LiClO_4$ concentration is shown in the inset of Fig. 12. This behaviour may be explained on the basis of weakening of the C=O bond that is due to the decrease in electron density due to

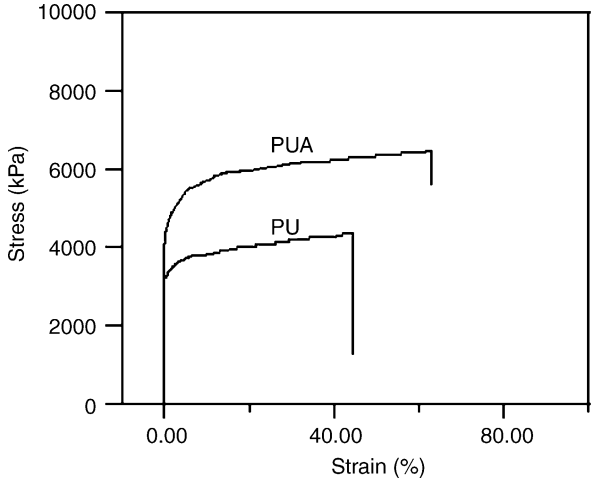

Fig. 11. Tensile behaviour of PU and PUA films (modulus, 500 kPa).

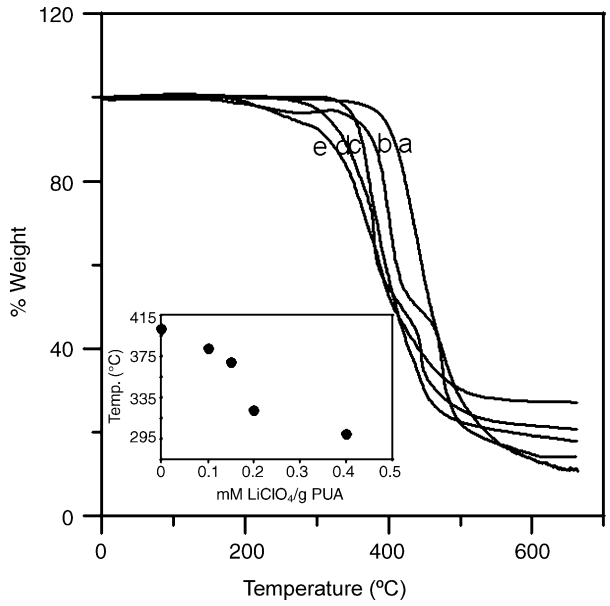

Fig. 12. Thermograms of PUA containing different amount of $LiClO_4$ concentrations. (a) Undoped PUA, (b) 0.10 mM $LiClO_4$ g^{-1} PUA, (c) 0.15 mM $LiClO_4$ g^{-1} PUA, (d) 0.20 mM $LiClO_4$ g^{-1} PUA and (e) 0.40 mM $LiClO_4$ g^{-1} PUA (inset: plot of decomposition temperature (T_d) vs. $LiClO_4$ concentration).

the interaction of Li^+ ions with the oxygen atoms [23]. Alternatively, perchlorate oxidation of the PEG phase can cause this thermal event starting from ~400 °C. The observed trend in thermal transitions at higher $LiClO_4$ concentration may arise from predominant oxidation of perchlorate.

3.10. Gel electrolytes

PUA can take up liquid plasticizer (LP-20) to different extents with time of contact between the polymer film and the plasticizer. The dimensional stability of the aforementioned gelatinous electrolyte is found to be very good for practical use. Generally, a plasticizer hinders the degree of crystallization of the polyurethane, and thus reduces the energy barrier for transportation of carrier ions and enhances the corresponding ionic conductivity. As the conductivity of PUA electrolytes was still on the lower side, gel polymer electrolytes (GPEs) were prepared to increase the conductivity by increasing the liquid electrolyte content. The GPEs were prepared via the dipping of dry polymer films into a commercial liquid electrolyte (LP-20). Swelling was continued until the swollen percentage reached the required value.

The temperature dependence of the conductivity of a gelatinous electrolyte of PUA is presented in Fig. 13(A). The gel electrolyte are found to follow an Arrhenius relationship. The conductivity of the gelled PUA at 30 °C is about 0.75×10^{-4} S cm^{-1}. A comparison of the conductivities of the parent PUA and the gelled PUA with equivalent concentrations of the $LiClO_4$ reveals that the difference in conductivity is 1 decade. The improvement in conductivity given by the matrix polymer domains may be low in comparison with that given by the plasticizer-rich domains. An enhancement in the number of

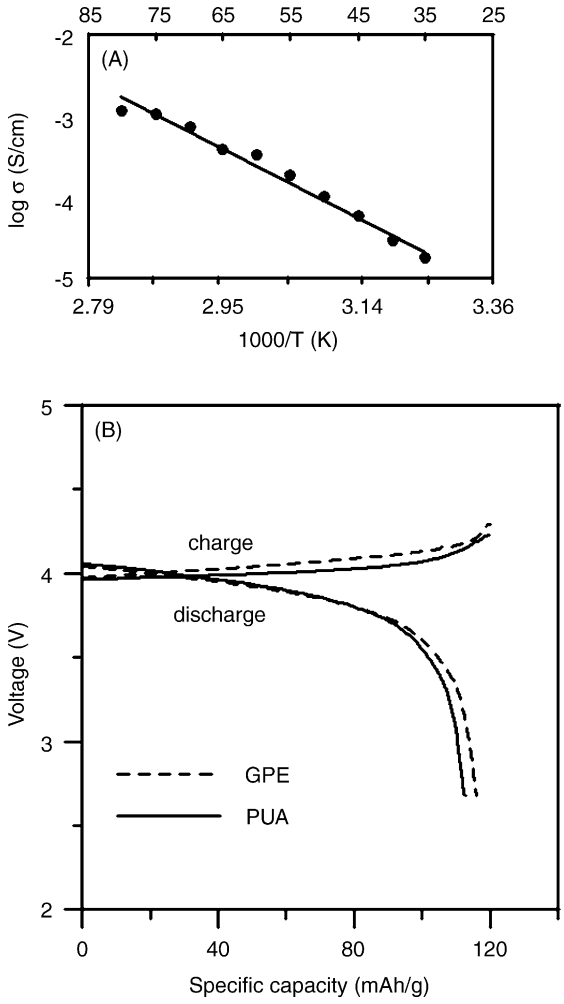

Fig. 13. (A) Temperature dependence of ionic conductivity of gelled PUA. (B) Charge–discharge performance of Li/PE(PUA)/$LiCoO_2$ and Li/(PUA-Gel)/$LiCoO_2$.

charge carriers is expected because of the solvation of some of the Li^+ ions by the matrix polymer.

3.11. Charge–discharge cycling tests

In order to investigate the utility of the PUA-based polymer electrolyte in a lithium-ion polymer battery, a cell was assembled with lithium metal as the anode and $LiCoO_2$ as the cathode. The theoretical capacity of the $LiCoO_2$ electrode is 120 mAh g^{-1}. A cycling test was performed at the C/10 rate and with cut-off voltages of 4.2 and 2.6 V for the upper and lower limits. The depth-of-discharge was restricted to ~120 mAh g^{-1} of $LiCoO_2$ in order to provide a high cycling performance.

The charge–discharge performance of Li/PUA/$LiCoO_2$ and Li/(PUA-Gel)/$LiCoO_2$ cells on the first cycle is shown in Fig. 13(B). The cells achieve a capacity of 112 mAh g^{-1}. Comparison of the discharge curves for both electrolytes reveals that the capacity of PUA electrolyte is slightly lower than that of gel electrolyte. The reduced capacity is due to the lower diffusion rate of lithium ions in PUA as compared with its gel electrolyte.

4. Conclusions

A cross-linked PUA is synthesized by end-capping HDI and PEG-based prepolymer with HBMA. The formation of transient cross-links with the ether oxygen of the soft segment and the mixing of soft and hard phases induced by the Li^+ ions are evident from DSC measurements. Also, the results from FT-IR spectroscopy and TGA measurements support the formation of different types of complexes by the interaction of Li^+ ions with different coordination sites of PUA. The PUA systems follow an Arrhenius relationship for ion transport and this implies that ion movement occurs by an activated hopping mechanism. Predominant formation of contact ion-pairs of $LiClO_4$ is observed by means of a.c. conductivity and DSC measurements. The PUA shows electrochemical stability up to 5.35 V versus Li/Li^+ and posseses better compatibility with lithium metal as inferred from impedance measurements. Addition of HBMA to the PU matrix improves the tensile strength of the cross-linked PUA. Swelling measurements of PUA with plasticizer show better dimensional stability. The conductivity of gelled PUA at 30 °C is about 0.75×10^{-4} S cm^{-1}. Also, a cell is constructed using PUA as electrolyte and its performance is assessed.

References

[1] S.W. Choi, S.M. Jo, W.S. Lee, Y.R. Kim, Adv. Mater. 15 (2003) 2003.
[2] J. Jiang, A. Kucernak, J. Electroanal. Chem. 567 (2004) 123.
[3] C.H. Yang, L.W. Chong, L.M. Huang, Y.L. Lee, T.C. Wen, Mater. Chem. Phys. 91 (2005) 15.
[4] J.S. Do, K.J. Wu, Sens. Actuators B 67 (2000) 209.
[5] M.B. Armand, J.M. Chabagno, M. Duclot, Proceedings of the Second International Meeting on Solid Electrolytes, St. Andrews, Scotland, 20–22 September, 1978.
[6] M.A.B. Meador, V.A. Cubon, D.A. Scheiman, W.R. Bennett, Chem. Mater. 15 (2003) 3018.
[7] S. Seki, Y. Kobayashi, H. Miyashiro, Y. Mita, T. Iwahori, Chem. Mater. 17 (2005) 2041.
[8] H.S. Lee, X.Q. Yang, J. McBreen, Z.S. Xu, T.A. Skotheim, Y. Okamoto, J. Electrochem. Soc. 141 (1994) 886.
[9] J. Barthel, R. Buestrich, E. Carl, H.J. Gores, J. Electrochem. Soc. 141 (1996) 3565.
[10] I. Nicotera, L. Coppola, C. Oliviero, A. Russo, G.A. Ranieri, Solid State Ionics 167 (2004) 213.
[11] H.S. Min, J.M. Ko, D.W. Kim, J. Power Sources 19 (2003) 469.
[12] J.R. Kim, S.W. Choi, S.M. Jo, W.S. Lee, B.C. Kim, Electrochim. Acta 50 (2004) 69.
[13] J. Vondrak, J. Reiter, J. Velicka, B. Klapste, M. Sedlarikova, J. Dvorak, J. Power Sources, in press.
[14] A.K. Hjelm, T. Eriksson, G. Lindbergh, Electrochim. Acta 48 (2002) 171.
[15] T.C. Wen, H.H. Kuo, A. Gopalan, Macromolecules 34 (2001) 2958.
[16] H.L. Wang, H.M. Kao, M. Digar, T.C. Wen, Macromolecules 34 (2001) 529.
[17] H.L. Wang, H.M. Kao, T.C. Wen, Macromolecules 33 (2000) 6910.
[18] W.C. Chen, H.H. Chen, T.C. Wen, M. Digar, A. Gopalan, J. Appl. Polym. Sci. 91 (2004) 1154.
[19] A. Pattanayak, S.C. Jana, Polymer 46 (2005) 5183.
[20] C.S. Kim, B.H. Kim, K. Kim, J. Power Sources 84 (1999) 12.
[21] S. Velankar, J. Pazos, S.L. Copper, J. Appl. Polym. Sci. 62 (1996) 1361.
[22] J. Sun, D.R. Mac Farlane, M. Forsyth, Solid State Ionics 85 (1996) 137.
[23] M. Digar, S.L. Hung, H.L. Wang, T.C. Wen, A. Gopalan, Polymer 43 (2002) 681.
[24] M. Digar, S.L. Hung, H.L. Wang, T.C. Wen, A. Gopalan, Polymer 43 (2002) 1615.
[25] P.G. Bruce, C.A. Vincent, J. Electroanal. Chem. Interfacial Electrochem. 225 (1987) 1.
[26] J.V. Van Bogart, P.E. Gibson, S.L. Copper, J. Polym. Sci. Polym. Phys. 12 (1983) 65.
[27] J.T. Koberstein, T.P. Russell, Macromolecules 19 (1986) 714.
[28] M. Watanabe, S. Oohashi, K. Sanui, T. Kobayashi, Z. Ohtaki, Macromolecules 18 (1985) 1945.
[29] I. Albinsson, B.E. Mellander, J.R. Stevens, J. Chem. Phys. 96 (1992) 681.
[30] S. Schantz, L.M. Torell, J.R. Stevens, J. Chem. Phys. 94 (1991) 6862.
[31] R. Seymour, S. Copper, Macromolecules 6 (1973) 48.
[32] G.A. Senich, W.J. Mac Knight, Macromolecules 13 (1980) 106.
[33] H.S. Lee, Y.K. Wang, S.L. Hsu, Macromolecules 20 (1987) 2089.
[34] J. Li, I.M. Khan, Macromolecules 26 (1993) 4544.
[35] W. Wieczorek, A. Zalewska, D. Raducha, Z. Florjanczyk, J.R. Stevens, A. Ferry, P. Jacobson, Macromolecules 29 (1996) 143.
[36] M. Solomon, M. Xu, E.M. Eyring, S.J. Petrucci, Phys. Chem. 98 (1994) 8234.
[37] M.M. Coleman, K.H. Lee, D.J. Skrovanek, P.C. Painter, Macromolecules 19 (1986) 2149.
[38] M.M. Coleman, D.J. Skrovanek, P.C. Painter, Macromolecules 18 (1985) 299.
[39] C.J. Pouchert (Ed.), The Aldrich Library of Infra-Red spectra, 1978.
[40] J.D. van Heumen, J.R. Stevens, Macromolecules 28 (1995) 4268.
[41] J. Herranen, J. Kinnuen, B. Mattsson, Solid State Ionics 80 (1995) 201.
[42] A. Ferry, G. Oradd, P. Jacobson, J. Chem. Phys. 108 (1998) 7426.
[43] F.M. Gray, Polymer Electrolytes, Springer, New York, 1997.
[44] M.H. Cohen, D. Turnbull, J. Chem. Phys. 31 (1959) 1164.
[45] Z.L. Peng, B. Wang, S.Q. Li, S. Wang, H. Liu, H.Q. Xie, Phys. Lett. A 194 (1994) 228.
[46] P.G. Bruce, C.A. Vincent, J. Electroanal. Chem. 225 (1987) 1.
[47] J.B. Goodenough, Solid State Ionics 69 (1994) 184.
[48] K.M. Abraham, A. Alamgir, Chem. Mater. 3 (1991) 339.
[49] Y. Matsuda, M. Morita, H. Tsutsumi, Polym. Adv. Technol. (1993) 209.
[50] F. Croce, F. Gerance, G. Dautzenberg, S. Passerini, G.B. Appetecchi, B. Scrosati, Electrochim. Acta 39 (1994) 2187.
[51] G.B. Appetecchi, F. Croce, B. Scrosati, Electrochim. Acta 40 (1995) 991.
[52] T. Mani, R. Mani, J.R. Stevens, Solid State Ionics 60 (1993) 113.
[53] R. Mani, T. Mani, J.R. Stevens, J. Polym. Sci., Part A: Polym. Chem. 30 (1992) 2025.
[54] G.B. Appetecchi, F. Croce, B. Scrosati, J. Power Sources 66 (1997) 77.
[55] S. Slane, N. Salomon, J. Power Sources 55 (1995) 7.
[56] G.B. Appetecchi, F. Croce, A. de Paolis, B. Scrosati, J. Electroanal. Chem. 463 (1999) 248.